Supplemental information

In-Situ Crosslinked Matrix enables Efficient and Mechanically Robust Organic Solar Cells with Frozen Nano-Morphology and Superior Deformability

Wei Song[1,2], *Zhenyu Chen*[1,2], *Congqi Lin*[1,2], *Pilan Zhang*[3], *Dinghong Sun*[1,2], *Weifu Zhang*[1,2], *Jinfeng Ge*[1,2], *Lin Xie*[1,2], *Ruixiang Peng*[1,2]*, *Daobin Yang*[1,2]*, *Quan Liu*[1,2], *Yifei Xu*[3], *Ziyi Ge*[1,2]*

[1]Zhejiang Engineering Research Center for Energy Optoelectronic Materials and Devices, Ningbo Institute of Materials Technology & Engineering, Chinese Academy of Sciences, Ningbo 315201, P. R. China

[2]Center of Materials Science and Optoelectronics Engineering, University of Chinese Academy of Sciences, Beijing 100049, P. R. China

[3]State Key Laboratory of Molecular Engineering of Polymers and Department of Macromolecular Science, Fudan University, Shanghai, China

*Corresponding: pengrx@nimte.ac.cn, yangdaobin@nimte.ac.cn, geziyi@nimte.ac.cn

Supplemental Experimental Procedures

Materials

Donor monomer (4, 8-bis(5-(2-ethylhexyl)-3, 4-difluorothiophen-2-yl) benzo [1, 2-b: 4, 5-*b*'] dithiophene-2, 6-diyl) bis (trimethylstannane) and acceptor monomer 5, 8-bis (5-bromo-4-(2-butyloctyl) thiophen-2-yl) dithieno [3', 2': 3, 4; 2'', 3'': 5, 6] benzo [1, 2-*c*] [1, 2, 5] thiadiazole were purchased from Nanjing Zhi yan Technology Co., Ltd.

The PM6, BTP-eC9 and PDINN were purchased from Solarmer Materials Inc. The molecular weight and dispersity of PM6 are Mn: 36kDa and PDI: 2.5-2.7, respectively. Toluene was purchased from Zhengzhou Alfa Chemical Co., Ltd., pyridine, chloroform was commercially available from China National Medicines Corporation Ltd. PEDOT: PSS (Clevios P VP 4083) was obtained from J&K Chemicals Inc. The indium-doped tin oxide (ITO) glass was purchased from Suzhou Shang yang Solar Technology Co., Ltd. All reagents were directly used without any further treatment, meanwhile, all of reactions were carried out under a nitrogen atmosphere.

OSCs fabrication

Rigid device: The rigid device was fabricated with the conventional device structure of glass/ITO/4PADCB/Active layer/PDINN/Ag. The ITO-coated glass was cleaned with detergent and ultrasonicated in deionized water, acetone and ethyl alcohol for 20 min each. The cleaned ITO subsequently blow-dried by nitrogen and then treated by ultraviolet ozone for 35 minutes. The 4PADCB in ethanol solution was spin-cast onto the treated-ITO surface at 3000 rpm. for 30 s and then thermal annealing at 100 °C for 10 minutes in glove box. After annealing treatment, a chloroform solution containing the donors and acceptor was prepared to spin coating for fabricating active layer. The concentration of donor was 7 mg/mL with 0.3 wt.% 1,8-diiodooctane (DIO) and the D/A ratio was kept as 1:1.2. Subsequently, PDINN was dissolved in methyl alcohol solution (1 mg/mL) and spin-coated at 2000 rpm for 30 s. Finally, a 150 nm Ag electrode were deposited under the pressure of 3×10^{-5} Pa.

Flexible device: The flexible OSC was fabricated with the traditional sandwich structure: PEN/ITO/4PADCB/active layer /PDINN/Ag. To avoid distortion of the PEN by the spin coater, the ITO/PEN first was adhered onto a glass substrate of equal size by polydimethylsiloxane (PDMS) elastomer base, and then the normal spin coating process of the device is performed. The cleaned ITO/PET subsequently blow-dried by nitrogen and then treated by ultraviolet ozone for 35 minutes. The 4PADCB in ethanol solution was spin-cast onto the treated-ITO surface at 3000 rpm. for 30 s and then thermal annealing at 100 °C for 10 minutes in glove box. After that, the active layer and PDINN process conditions are the same as those of the rigid device. Finally, a 150 nm Ag electrode were deposited under the pressure of 3×10^{-5} Pa. The repeated bending cycle tests are performed by Mechanical Cyclic Deformation System.

Characterization and Measurements

Elemental analyses were carried out using an Elementar elemental analyzer. Spectrophotometer (Perkin-Elm er Lambda 950) was taken to test the UV-vis absorption spectrums. Grazing incidence wide-angle X-ray scattering (GIWAXS) was measured to research the molecular packing, crystallinity, and mode direction of the films.

Photovoltaic performances of the OSCs were performed via the solar simulator (Newport-Oriel® Sol3A 450W). The intensity of the AM 1.5G spectra was calibrated by a certified standard silicon solar cell.

Cyclic voltammetry (CV)

The energy levels for **D18-2F** were measured by cyclic voltammetry (CV) using a PC controlled 604E electrochemical workstation, which was performed by using Ag/AgCl as reference electrode in 0.1 mol L^{-1} tetra-*n*-butylammonium hexafluorophosphate (n-Bu4NPF$_6$) solution, and ferrocene/ferrocenium (Fc/Fc$^+$) (-0.1 eV versus Ag/AgCl) was used as internal reference. The CV system was constructed using a Pt disk as the working electrode, a Pt wire as the counter electrode, and an Ag/AgNO$_3$ (0.1 mol L^{-1} in acetonitrile) electrode as the reference electrode. The HOMO and LUMO were

calculated according to the following equations:

$$E_{HOMO/LUMO} = -\left(\varphi_{ox/red} - \varphi_{Fc/Fc^+} + 4.8\right) eV$$

Where φ_{ox} is the onset of oxidation and the φ_{red} relates to the reduction potential, respectively.

Peak force quantitation nanomechanical mapping (PFQNM) characterizations

The Derjaguin-Muller-Toporov (DMT) modulus, adhesion, deformation, and atomic force microscope (AFM) images were obtained from PFQNM and tapping mode by a Veeco Dimension 3100V atomic force microscope.
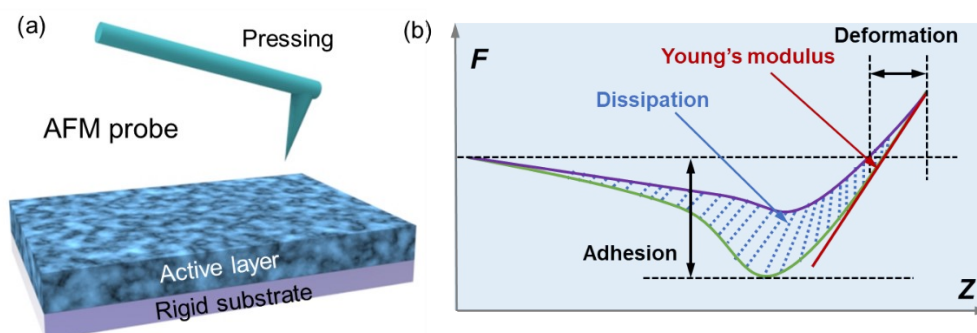
Figure S1. (a) Schematic diagram of the AFM PFQNM technology. (b) Schematic diagram of a full force-distance curve. The Young's modulus can be extracted by extrapolating the linear portion of the retraction curve after the contact point. The adhesion is the vertical distance between the base line and the bottom most part of the retraction curve.

Pseudo free-standing tensile test

Stress-strain curves were tested on in-situ micro-mechanical testing system (**PR-MMT6SL-100F**, Shenzhen HuaJason Technologies, Co., LTD.). The films were spin-casted onto the PEDOT: PSS (4083)-coated glass substrate at first, and then cut into long strips approximately 5 mm wide and 20 mm long to assemble the sample. Afterward, the films were floated onto the water surface, and attached to the grips by van der Waals forces. The strain was applied at a fixed strain rate, and the tensile load values were measured by a load cell with high resolution.

In-situ ultraviolet-visible (UV-vis) absorption

In-situ UV-vis absorption measurements were performed by the Filmetrics F20-EXR spectrometer using the transmission mode with a time resolution of 0.1 s.[1] The spectrometer consists of a light source and detector. The light source and detector are fixed above and below the substrate, respectively, and on the same vertical line. The solution was injected into the slot, and the film was coated onto the glass substrate. The detector collects the transmission spectra ranging from 400 to 1050 nm during coating. The UV-vis absorption spectra are calculated from the transmission spectra according to the equation $A_\lambda = -\log_{10}(T)$, where A_λ is the absorbance at a certain wavelength (λ), and T is the calculated transmittance. The light source and detector were turned on before coating the film, so time zero is the point when the first solution transmission spectrum was collected by the detector. Before time zero, there is only noise in the transmission spectra.

In-situ photoluminescence spectra

In-situ Photoluminescence Spectra Measurements were performed by a laser device (MGL-III-785-300mW BH81223) with a time resolution of 0.1 s.

Cryogenic transmission electron microscopy (cryo-TEM)

For sample preparation, 6 μL solution was dropped on a Cu Quantifoil holey carbon grid, and the excess solution was blotted for 1 s by a filter paper. Then, the grid was immediately plunged into liquid ethane with ThermoFisher Vitrobot™ Mark IV (4°C and 20% humidity). Next, the grid was transferred into a JEOL CryoARM cryo-TEM equipped with a cold field emission gun operating at 300 kV, an Omega energy filter, and a Gatan K3 direct electron detector. Images were recorded with a defocus value of ~−3 μm.

Space charge limited current measurements (*SCLC*)

The carrier mobilities were measured by SCLC method. The electron-only devices were fabricated in a structure of ITO/Al/active layer/PDINN/Ag, whereas hole-only devices were fabricated utilizing a structure of ITO/PEDOT:PSS/active layer/MoO_3/Ag. The charge mobilities were determined by fitting the dark current measurement curves according to the Motto-Gurney law:

$$J_{SCLC} = \frac{9}{8}\varepsilon_0\varepsilon_r\mu\frac{V^2}{L^3}$$

where J_{SCLC} is the current density, ε_0 is the permittivity of free space (8.85×10^{-14} F/cm), ε_r is the relative dielectric constant of the BHJ systems (~3 for conjugated polymers), μ is the charge mobility. L is the thickness of the active layer, and V is the applied voltage in OSCs.

Contact angle measurement

Contact angles were measured from spin-coated films by an optical contact angle meter (CAM 200). The surface energy was estimated by the Harmonic mean equations:

$$(1 + \cos\theta_1)\gamma_1 = 2(\gamma_1^d\gamma_s^d)^{\frac{1}{2}} + 2(\gamma_1^p\gamma_s^p)^{\frac{1}{2}}$$

$$(1 + \cos\theta_2)\gamma_2 = 2(\gamma_2^d\gamma_s^d)^{\frac{1}{2}} + 2(\gamma_2^p\gamma_s^p)^{\frac{1}{2}}$$

$$\gamma_s = \gamma_s^d + \gamma_s^p$$

where γ_s^d represents the dispersive components, γ_s^p is the polar component, γ_s is the surface energy. θ_1 and θ_2 are the contact angles of pure water and glycerol, respectively.

H_2O: $\gamma_1 = 72.8$ mJ/m², $\gamma_1^d = 21.8$ mJ/m², $\gamma_1^p = 51.0$ mJ/m².

Diiodomethane: $\gamma_2 = 50.8$ mJ/m², $\gamma_2^d = 48.5$ mJ/m², $\gamma_2^p = 2.3$ mJ/m².

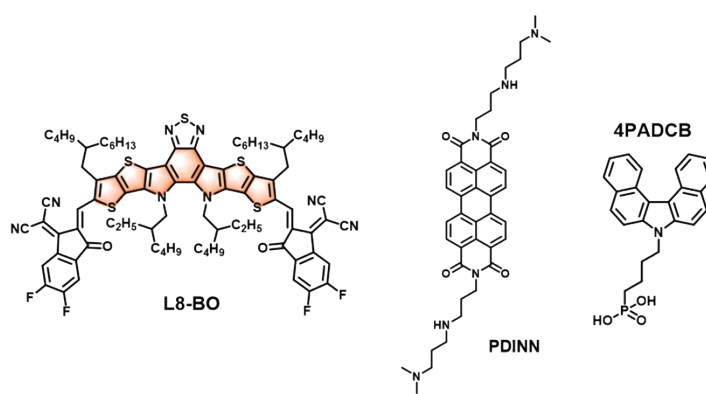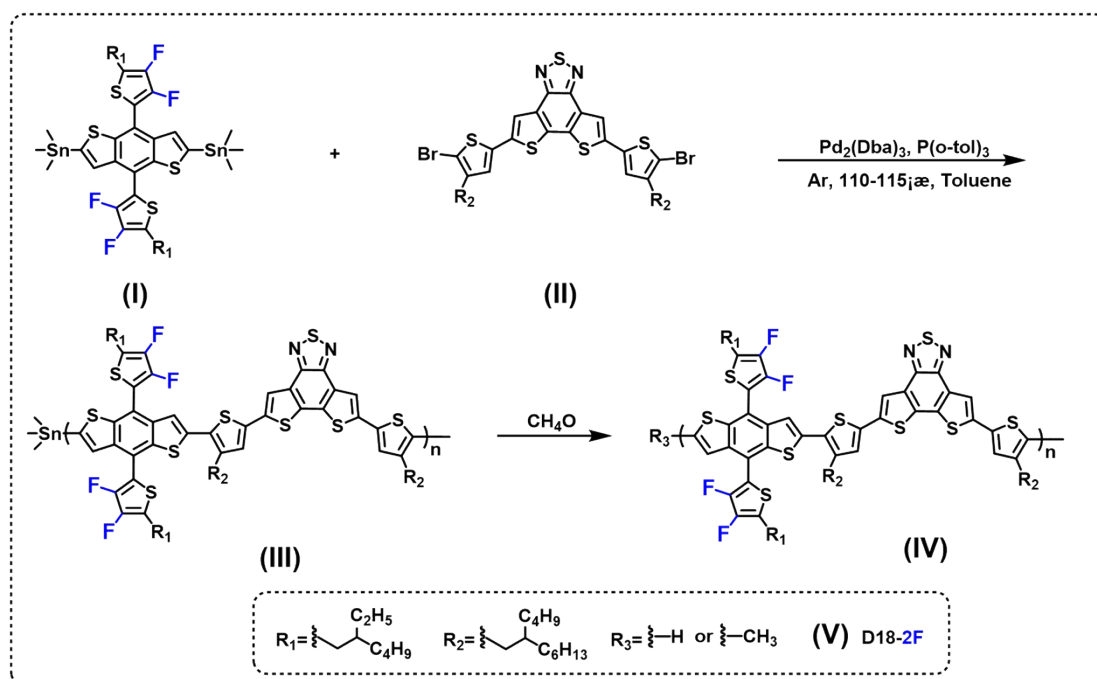## Supplemental Figures and Tables

Figure S2. Molecular structure of L8-BO, PDINN and 4PADCB.

The synthetic route of D18-2F

Scheme S1. The synthetic route of **D18-2F**.

Monomer (I): (4, 8-bis(5-(2-ethylhexyl)-3, 4-difluorothiophen-2-yl) benzo [1, 2-b: 4, 5-b'] dithiophene-2, 6-diyl) bis (trimethylstannane), molecular weight (M_w): 976.53 kg mol^{-1}, ^{1}H NMR (CDCl$_3$): δ 7.41 (d, J = 2.1 Hz, 2H), 2.79 (dd, J = 7.0, 3.0 Hz, 4H), 1.71 – 1.67 (m, 2H), 1.50 (d, J = 24.0 Hz, 4H), 1.35 (d, J = 6.6 Hz, 12H), 0.97 – 0.92 (m, 12H), 0.42 (s, 18H).

Monomer (II): 5, 8-bis (5-bromo-4-(2-butyloctyl) thiophen-2-yl) dithieno [3', 2': 3, 4; 2'', 3'': 5, 6] benzo [1, 2-c] [1, 2, 5] thiadiazole, M_w: 907.02, ^{1}H NMR (400 MHz, CDCl$_3$): 1H NMR (400 MHz, CDCl3) δ 7.87 (s, 2H), 6.96 (s, 2H), 2.51 (d, J = 7.2 Hz, 4H), 1.31 (d, J = 12.0 Hz, 33H), 0.91 (d, J = 8.8 Hz, 12H).

Synthesis of polymer donor (IV) D18-2F: **Monomer (I)** (100 mg, 0.1027 mmol), **monomer (II)** (93.17 mg, 0.1027 mmol), additive **Pd₂(Dba)₃** (10 mg, 0.0109 mmol) and additive **P(o-tol)₃** (10 mg, 0.03285 mmol) were dissolved in Toluene (1.5 ml) and stirred at 110°C for 10 h under nitrogen atmosphere. The solvent was removed under vacuum after the reaction mixture was cooled to ambient temperature and Settled in methanol. Afterward, D18-2F was purified through Soxhlet extraction, followed by acetone, methanol, dichloromethane, chloroform, and chlorobenzene. Finally, the components in chlorobenzene were collected and settled in methanol. The components in chlorobenzene were finally collected and settled in methanol. After overnight drying in a vacuum drying oven, a brownish yellow target product (131.36 mg, 68 % yield) was obtained. ^{1}H NMR (CDCl$_3$): δ = 7.52 (br, aromatic protons), 7.00 (br, aromatic protons), 6.38 (br, aliphatic protons), 3.00 (br, aliphatic protons), 1.26 - 0.55 (br, aromatic protons).
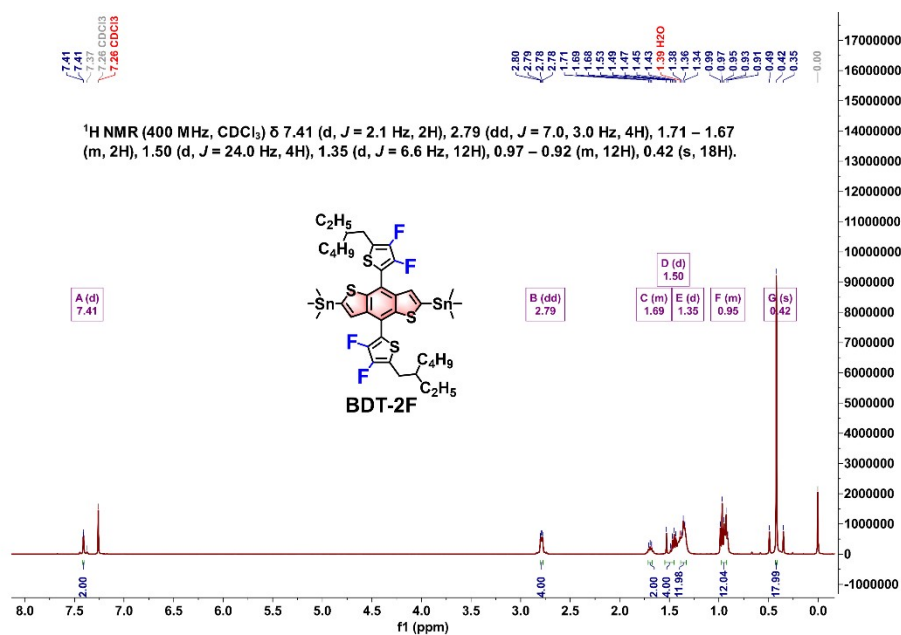
Figure S3. ^{1}H-NMR spectrum of **monomer (I)** in chloroform-*d*.

^{1}H NMR (400 MHz, CDCl$_3$) δ 7.87 (s, 2H), 6.96 (s, 2H), 2.51 (d, J = 7.2 Hz, 4H), 1.31 (d, J = 12.0 Hz, 33H), 0.91 (d, J = 8.8 Hz, 12H).
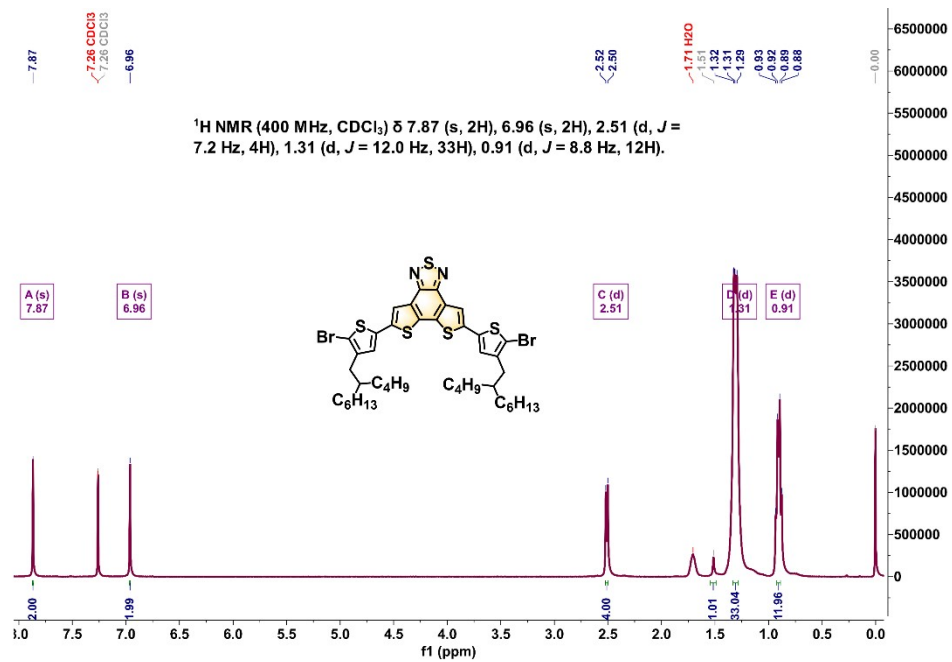
Figure S4. ^{1}H-NMR spectrum of **monomer (II)** in chloroform-*d*.

^{1}H NMR (400 MHz, CDCl$_3$) δ 7.52 (s), 7.00 (s), 6.38 (s), 3.00 (s), 1.26 (s), 0.95 (d, J = 53.0 Hz), 0.22 (s).
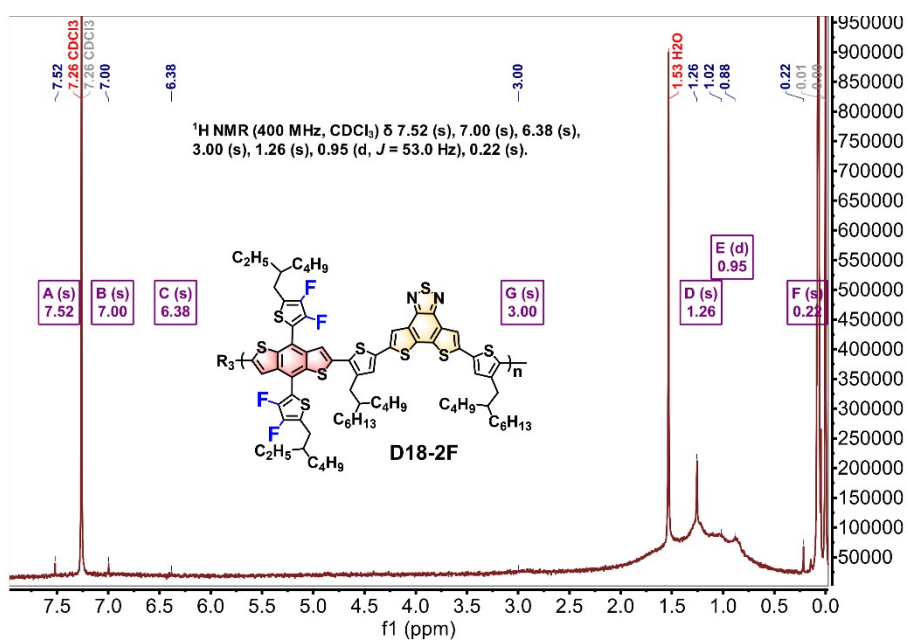
Figure S5. ^{1}H-NMR spectrum of **polymer donor (IV)** D18-2F in chloroform-*d*.
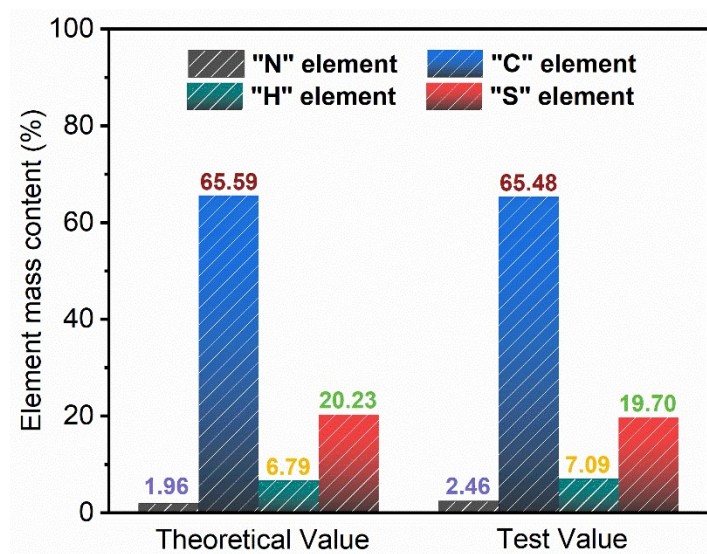
Figure S6. Elemental analysis characterization for **D18-2F**.

1. DFT theoretical calculations

The detailed theoretical calculations of **D18-2F** based on DFT theory at B3LYP/6-31G (d, p) level.

ESP (Top View)
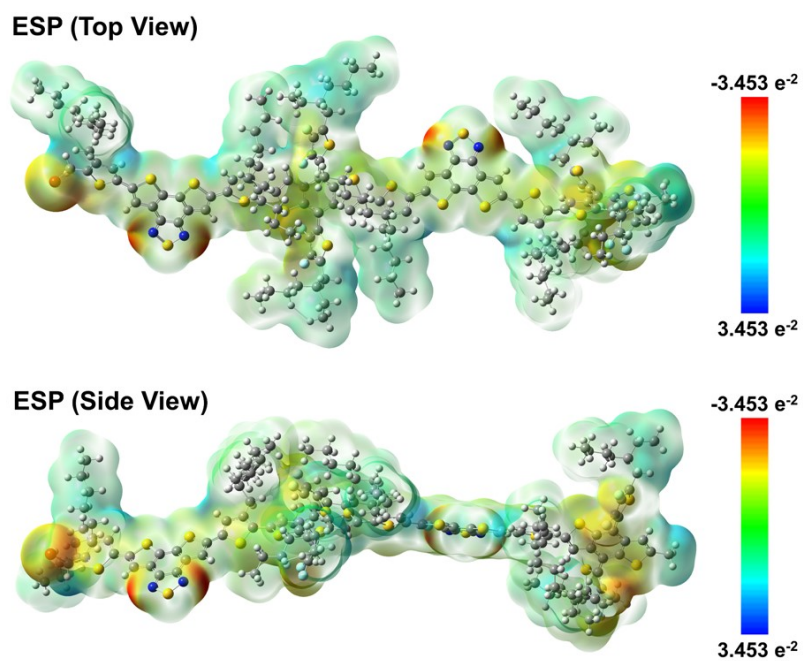
ESP (Side View)

Figure S7. ESP distribution of **D18-2F**.
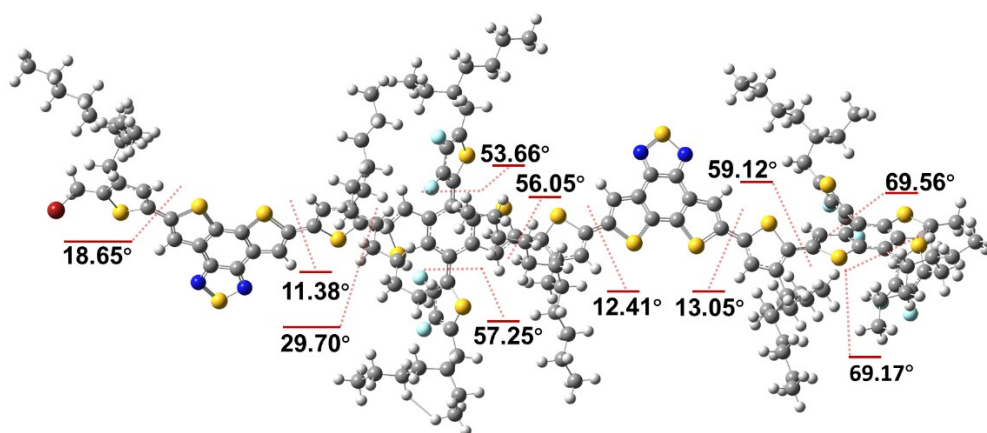
Figure S8. The twist dihedral angels of **D18-2F**.

HOMO = -5.06 eV
(Top View)
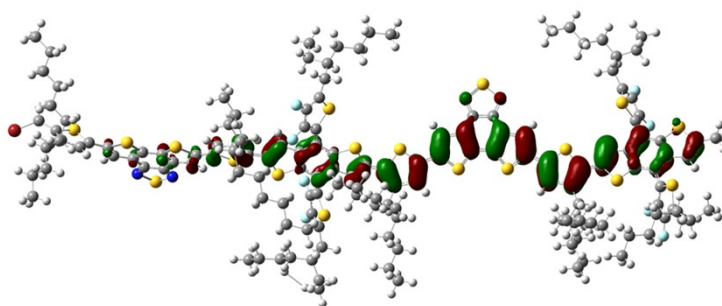
(Side View)
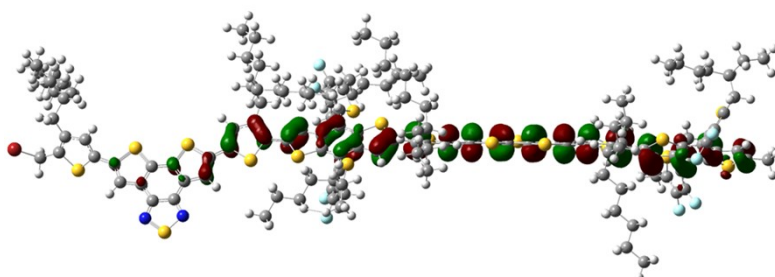
Figure S9. HOMO energy levels of D18-2F in top and side view.

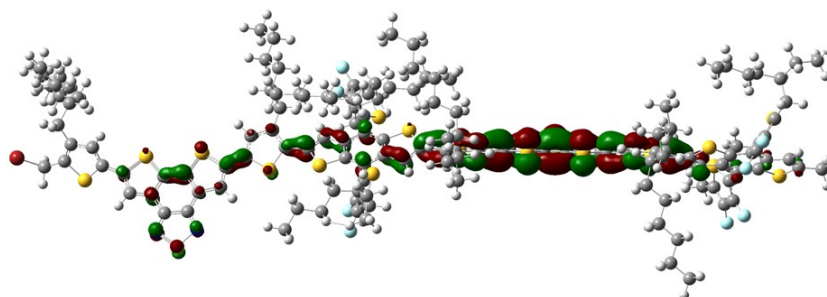**LUMO -2.53 eV**
(Top View)
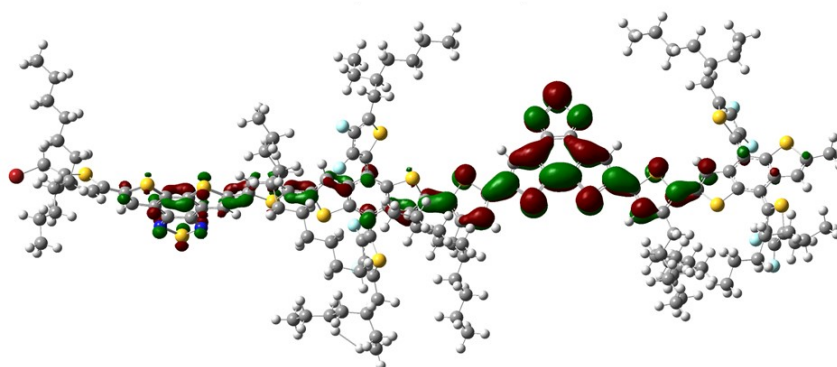
(Side View)

Figure S10. LUMO energy levels of D18-2F in top and side view.
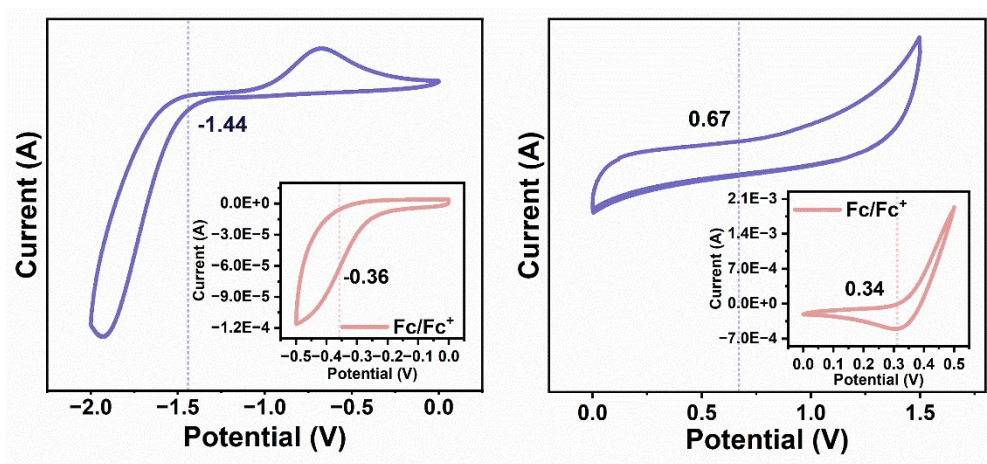
Figure S11. Electrochemical cyclic voltammetry curves of D18-2F.

GPC characterization

The Mn, Mw and PD were acquired on 1260 HT Infinity II in chloroform, with the solution of 3^{-1} mg ml^{-1}.
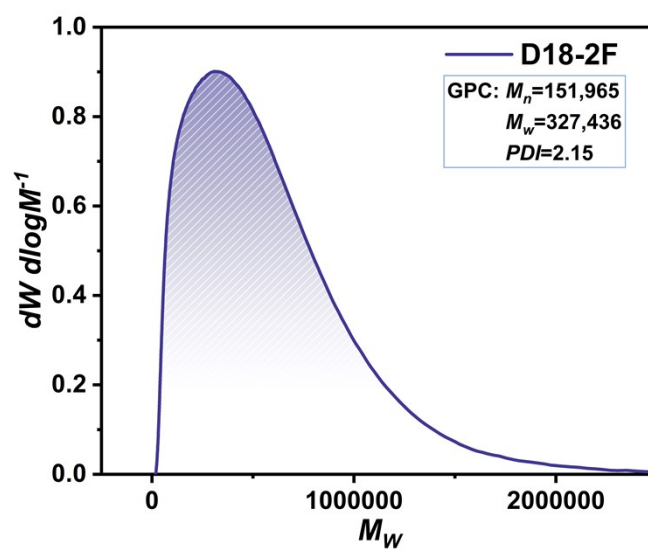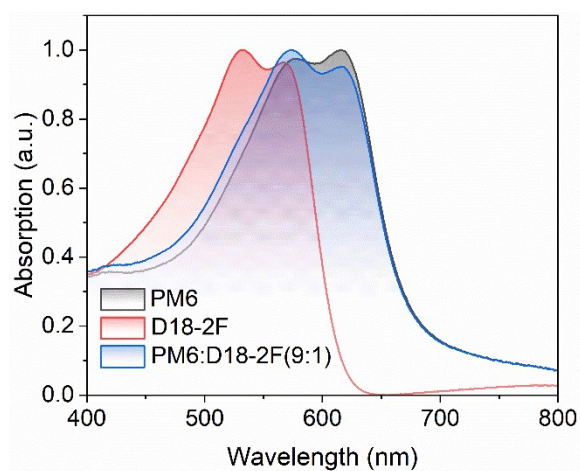

Figure S12. GPC test for D18-2F.

Figure S13. Normalized UV/Vis absorption spectra of PM6, D18-2F, and PM6:D18-2F (9:1) in films.
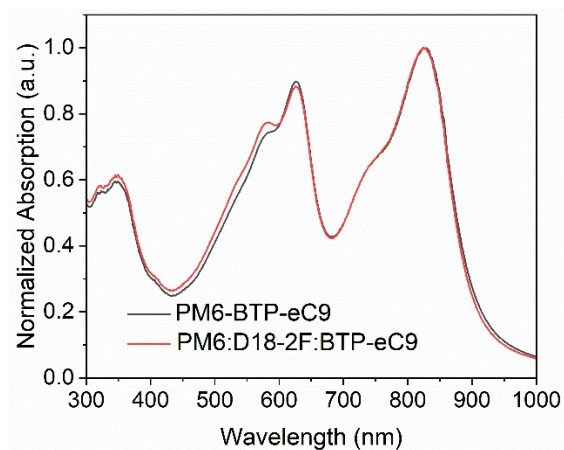

Figure S14. The normalized absorption of the PM6:BTP-eC9 and PM6:D18-2F:BTP-eC9 (0.9:0.1:1.2) on quartz substrate.
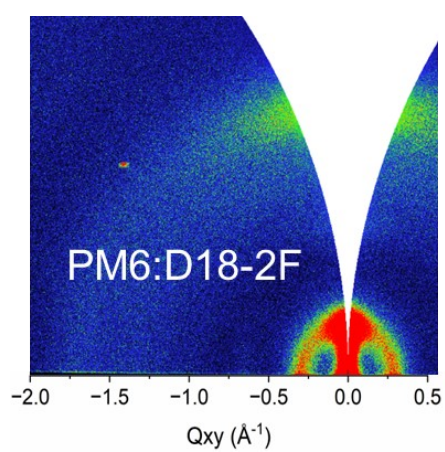

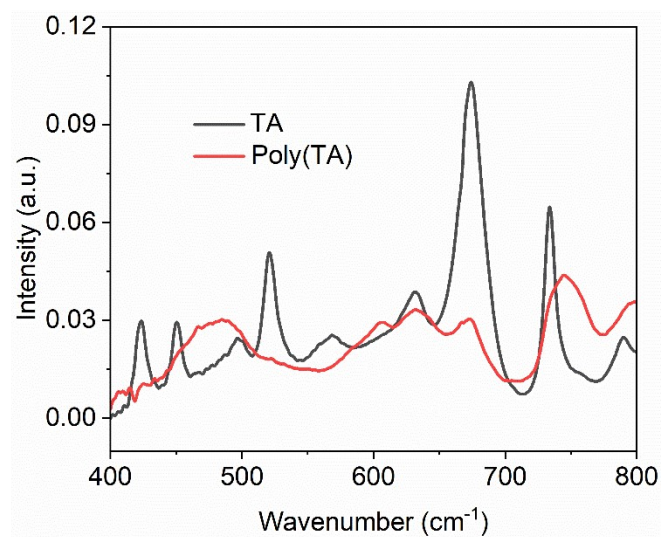**Figure S15.** 2D GIWAXS characterization for PM6:D18-2F (9:1) films.

Figure S16. Fourier transform infrared (FTIR) spectra TA and TA heating at 60°C.

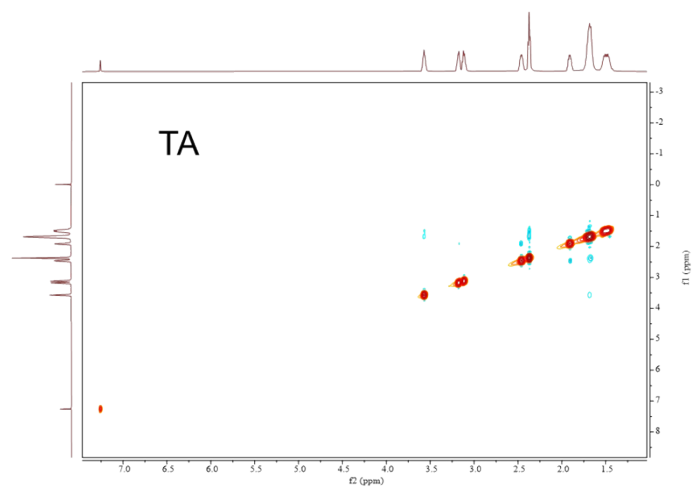**Figure S17**. 2D ^{1}H–^{1}H NMR spectra of TA in CDCl$_3$ solutions.
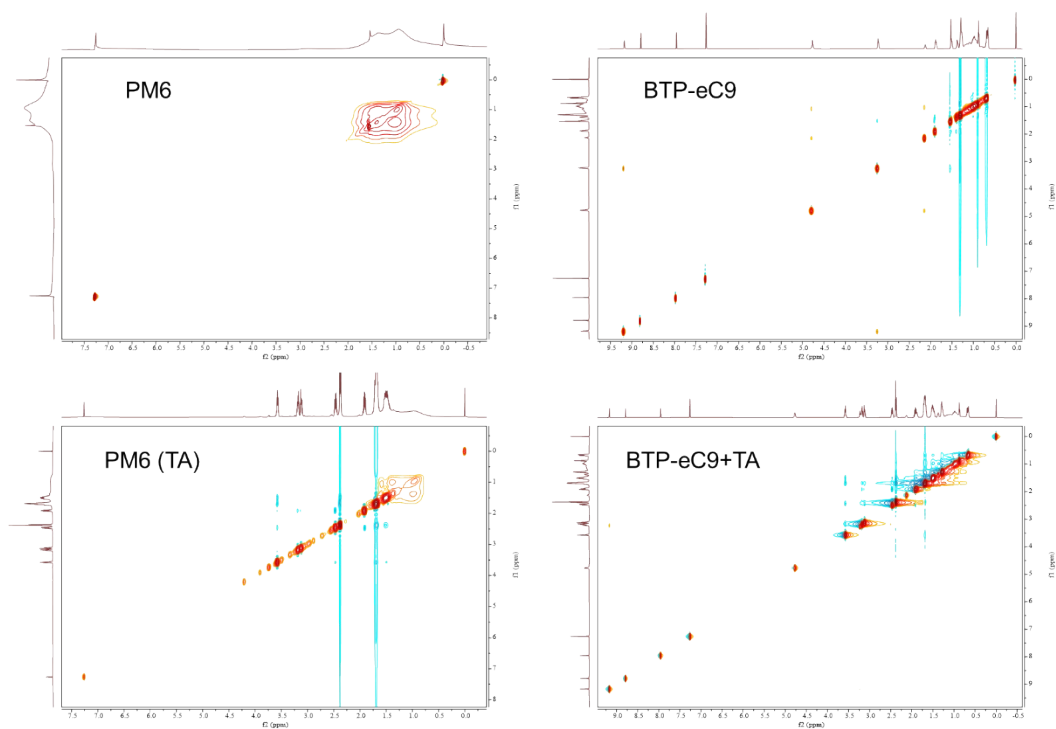
Figure S18. 2D ^{1}H–^{1}H NMR spectra of PM6, TA-doped PM6, BTP-eC9 and TA-doped BTP-eC9 in CDCl$_3$ solutions. The weight ratios were set as PM6:TA = 1:1, BTP-eC9:TA = 1:1.

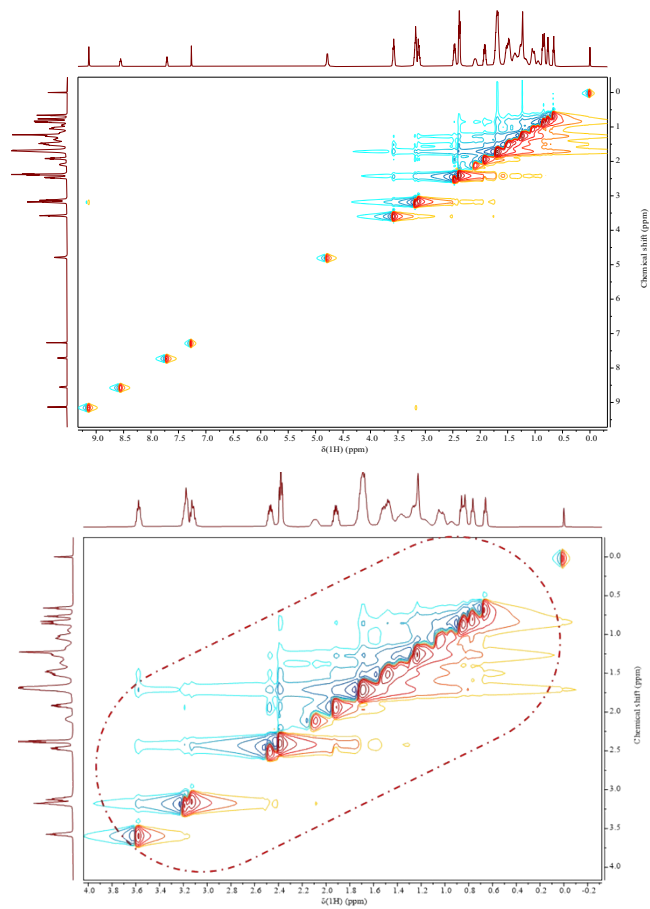**Figure S19**. 2D ^{1}H–^{1}H NMR spectra of L8-BO and TA-doped L8-BO in CDCl$_3$ solutions. The weight ratios were set as, L8-BO:TA = 1:1.
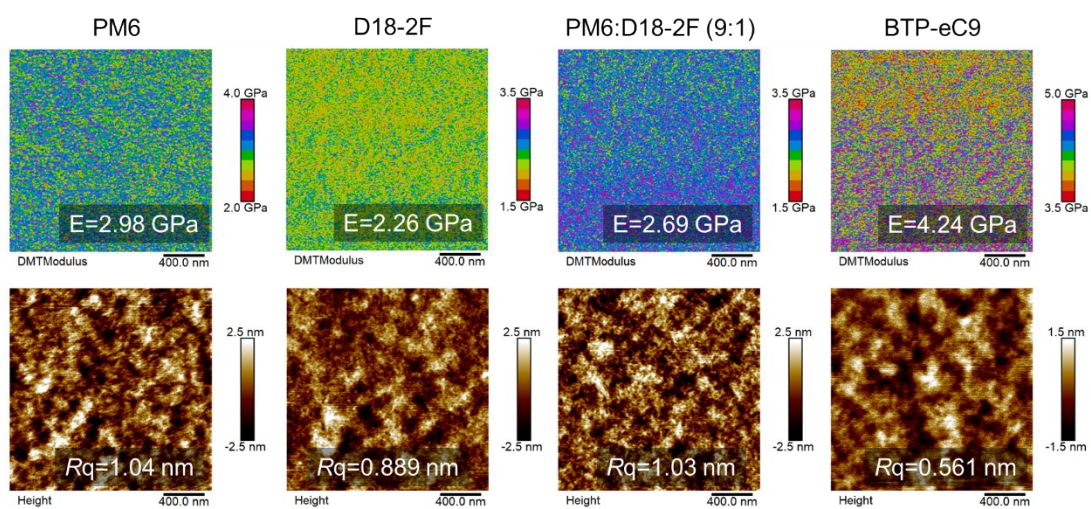
Figure S20. Derjaguin–Muller–Toporov (DMT) modulus and height images of PM6, D18-2F, PM6:D18-2F (9:1) and BTP-eC9 film.
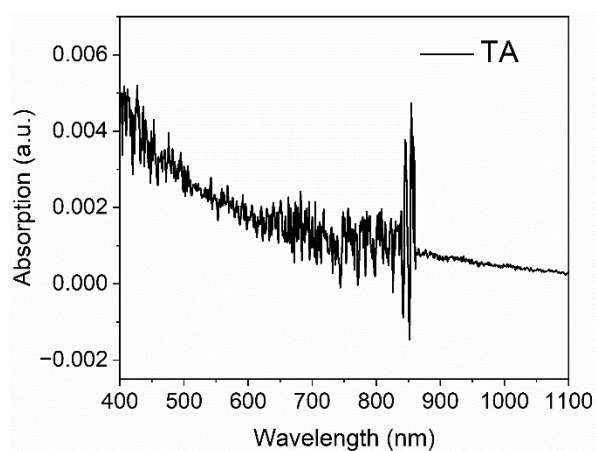
Figure S21. The optical absorption of the TA on quartz substrate.
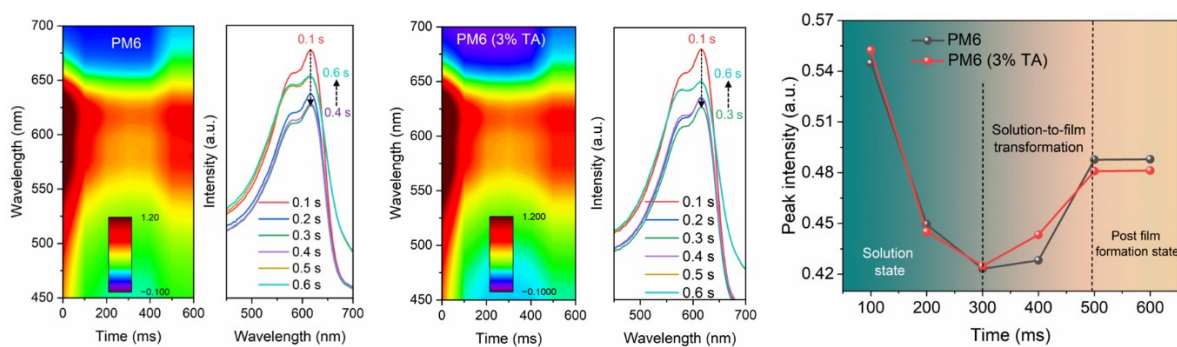
Figure S22. (a and b) The color mapping of *in-situ* UV-vis reflectance spectra as a function of spin-coating time, and in-situ UV-vis spectra during the first 0.6 s of spin coating process. (c) Normalized *in-situ* absorption intensity at the peak location of corresponding to acceptor films.
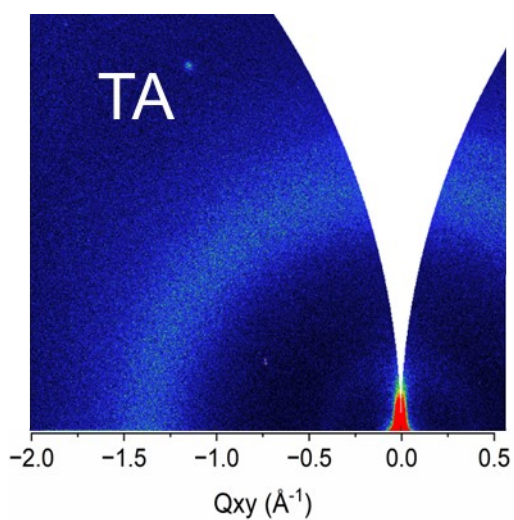
Figure S23. 2D GIWAXS characterization for TA films.
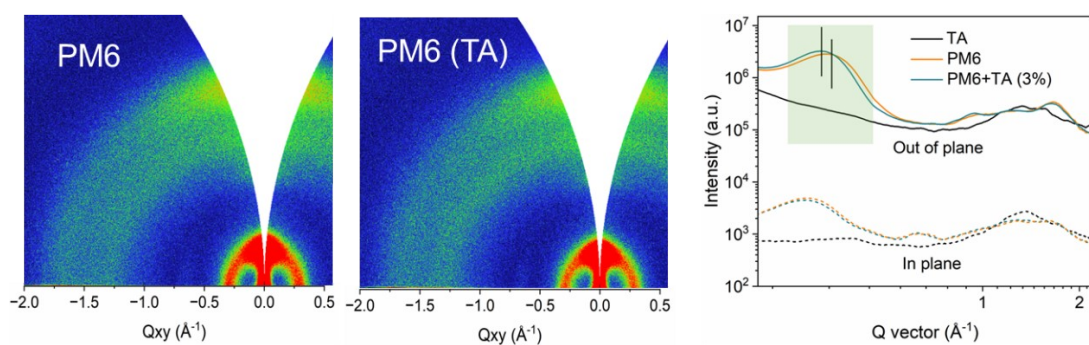
Figure S24. (a and b) 2D GIWAXS characterization for PM6 and TA-doped PM6 films. (c) 1D X-ray profiles along the OOP and IP linecut profiles of the 2D GIWAXS patterns of corresponding to films.
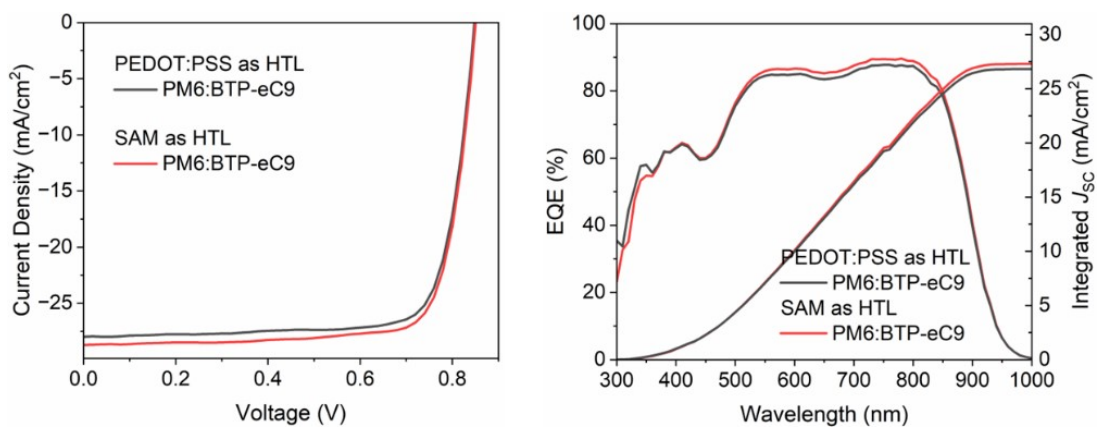
Figure S25. (a) *J–V* curves of the rigid devices fabricated with PM6:BTP-eC9 with PEDOT:PSS and SAM as hole transport layer. (b) EQE curves of the corresponding devices.
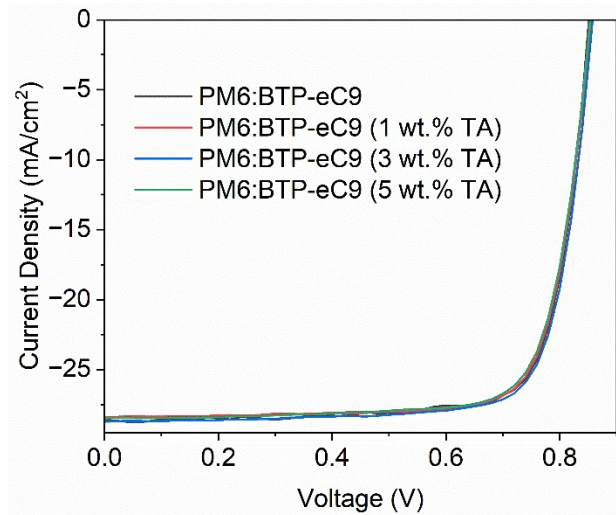
Figure S26. *J–V* curves of the PM6:BTP-eC9-based devices doped with different concentrations of TA.
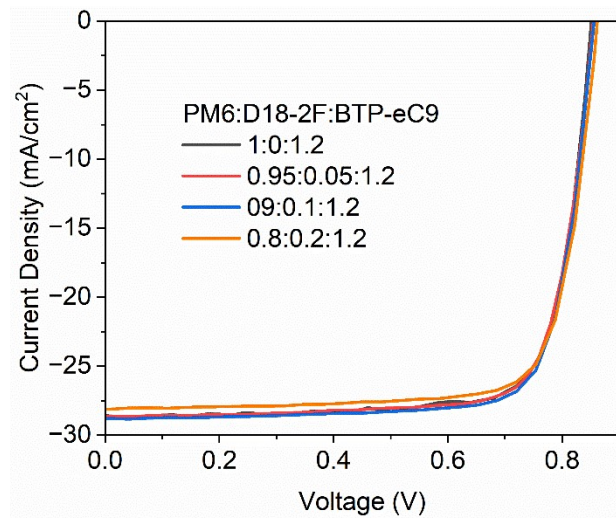
Figure S27. *J–V* curves of the PM6:D18-2F:BTP-eC9-based devices by varying the blending ratio of D18-2F.

Type	Single junction organic solar cell
Sample No.	DC2024a027
Area	0.0484 cm^2
Isc	1.387 mA
Jsc	28.667 mA/cm^2
Voc	0.863 V
FF	78.79 %
Pm	0.944 mW
E_{ff}	19.50 %
Ipm	1.276 mA
Vpm	0.740 V
Voltage Sweep	Forward
Sweep time	12.0 s
Temp	25 ℃
Irr	100 mW/cm^2
Curve	A20240329145411
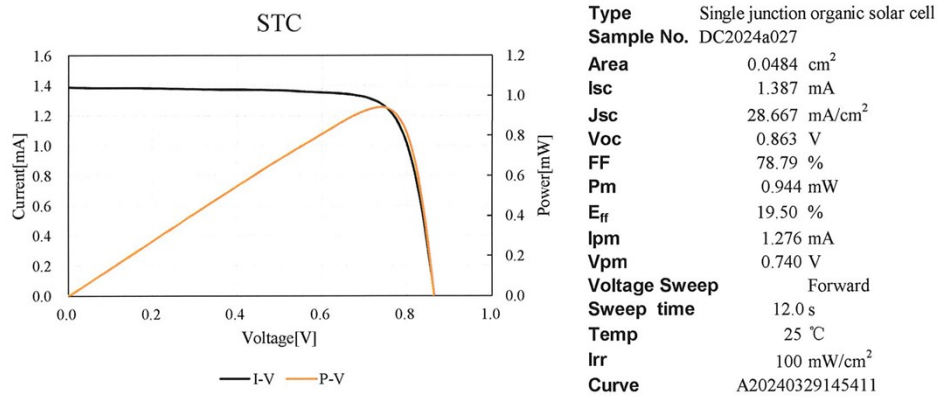
— End of Report —

Figure S28. PCE certified at Institute of Electrical Engineering, Chinese Academy of Sciences, showing an efficiency of 19.50% (Report No: PWQC-WT-P24032522-2R).
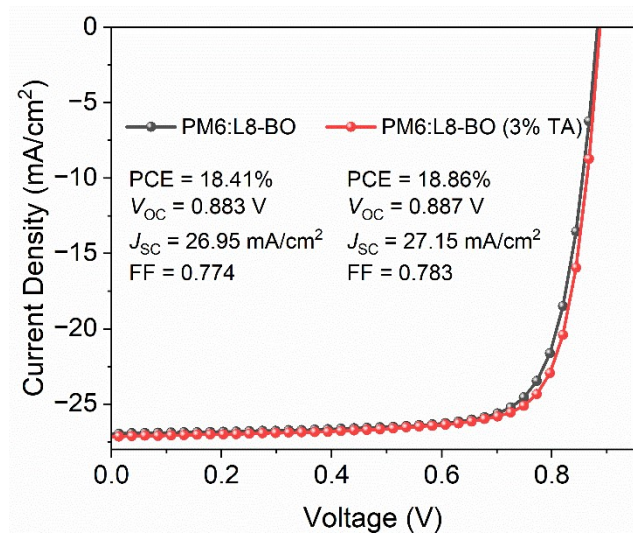
Figure S29. *J–V* curves of the PM6:L8-BO and 3 wt.% TA-doped PM6:L8-BO-based devices fabricated with PEDOT:PSS as hole transport layer.
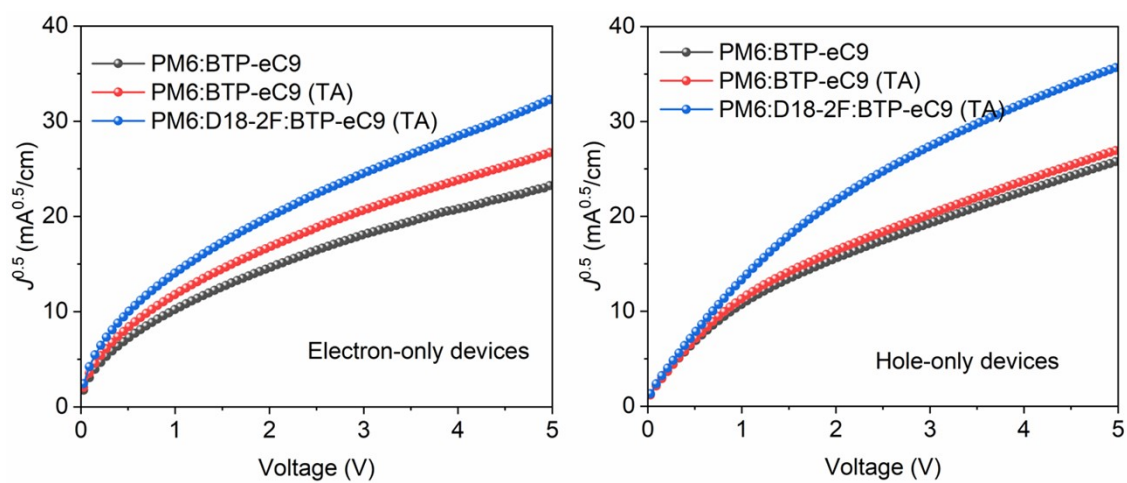
Figure S30. The electron (μ_e) and hole (μ_h) mobilities of the devices.
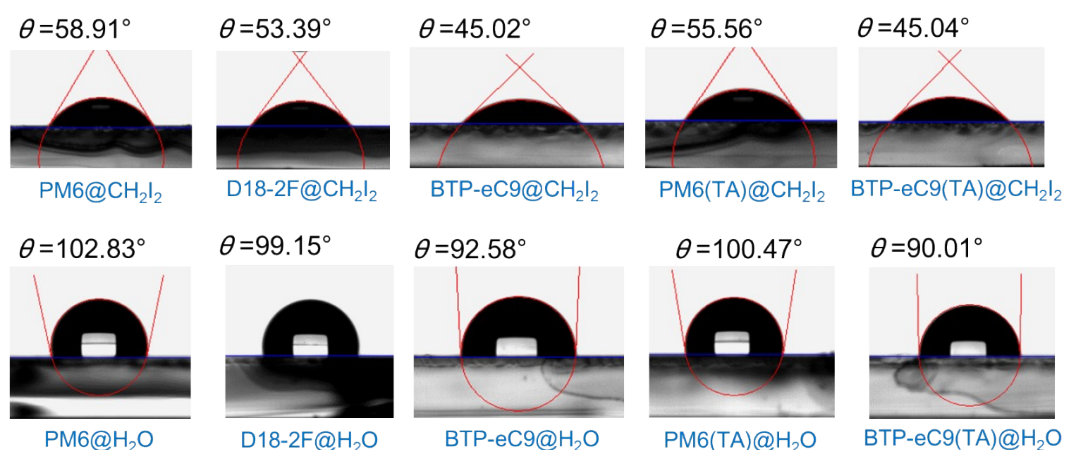
Figure S31. Contact angles of PM6, D18-2F, BTP-eC9, PM6 (TA) and BTP-eC9 (TA) thin films by applying deionized water (H_2O) and diiodomethane (DIM) liquid drops.

To determine the compatibility and miscibility of D18-2F, as shown in **Figure S30** and **Table S7**, the contact angles (CA) of water and diiodomethane liquid drops were evaluated. The corresponding surface energies (γ) were calculated using the Owens-Wendt-Rabel-Kaelble method. The γ values of PM6, D18-2F, and BTP-eC9 were 29.778 mN m^{-1}, 32.809 mN m^{-1}, and 37.141 mN m^{-1} respectively. In addition to similar surface energies, PM6 and D18-2F exhibit strong miscibility, as indicated by χ values (0.134κ K for D18-2F/BTP-eC9 and 0.073κ K for D18-2F/PM6), indicating that they

can form well-mixed donors.
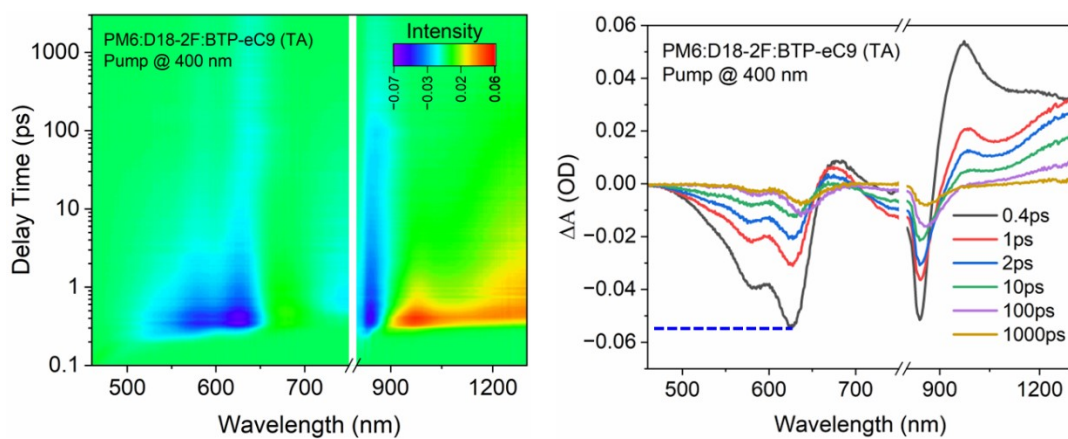
Figure S32. (a) 2D transient absorption image of the TA-doped PM6:D18-2F:BTP-eC9 with 400 nm excitation. (b) Absorption spectrum of corresponding to blend films at indicated delay times.
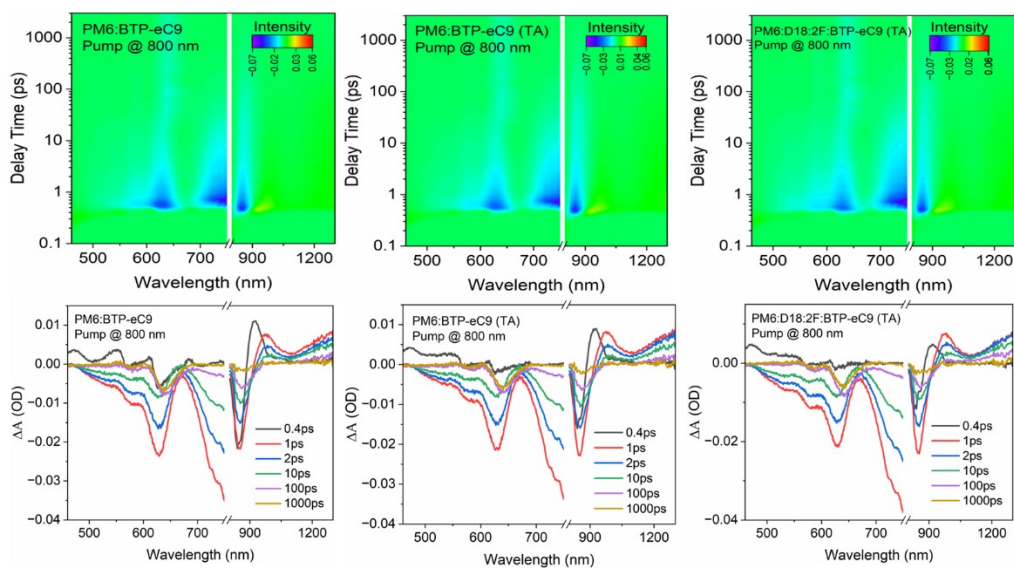
Figure S33. (a) 2D transient absorption image of the blend films with 800 nm excitation. (b) Absorption spectrum of corresponding to blend films at indicated delay times.
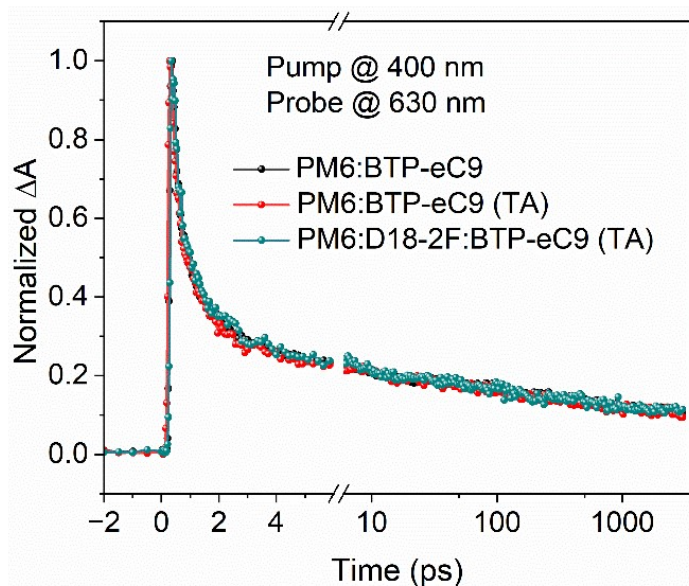
Figure S34. Decay kinetics of corresponding to blend films at 630 nm wavelength.
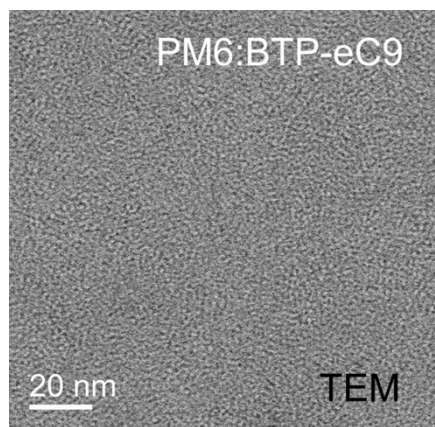
Figure S35. High-resolution TEM images of the PM6:BTP-eC9 films.
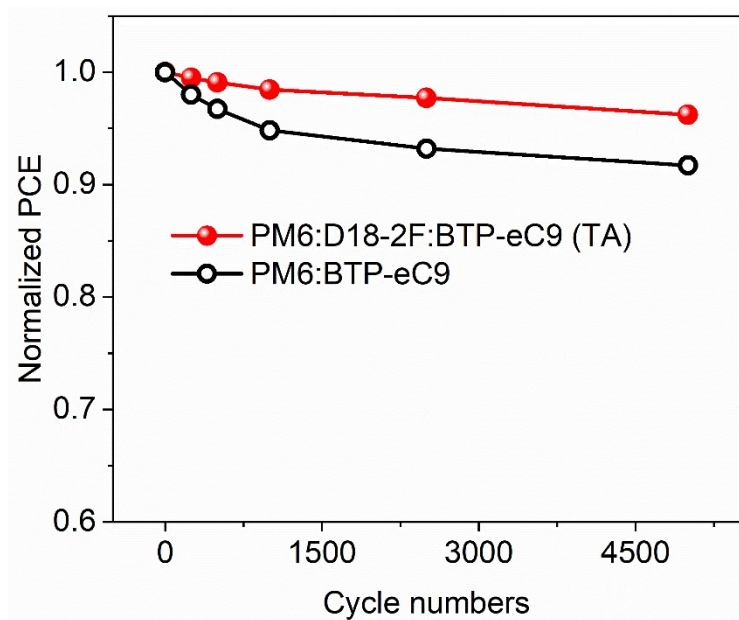
Figure S36. Decays of normalized PCEs of flexible devices in a continuous bending test.
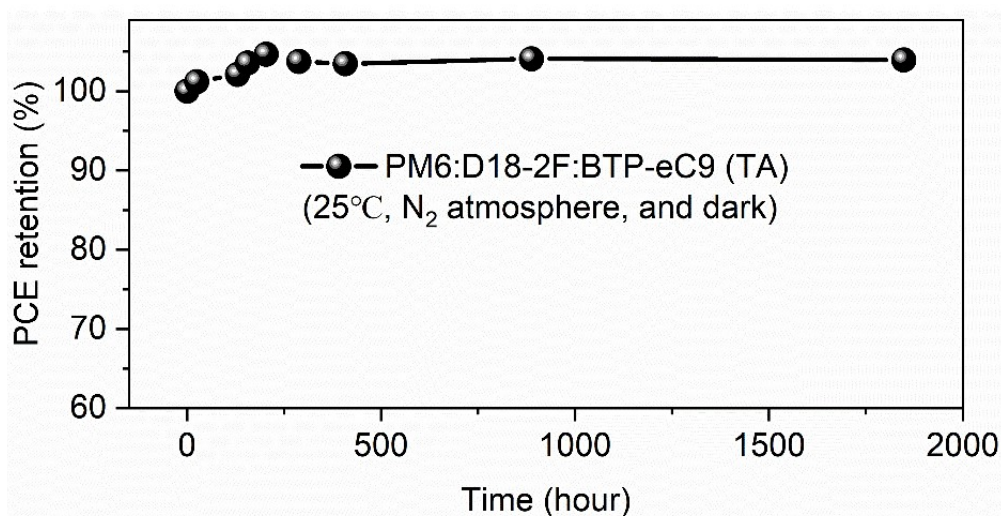
Figure S37. Shelf storage lifetime of inverted devices without encapsulation (25°C, N_2 atmosphere, and dark conditions).
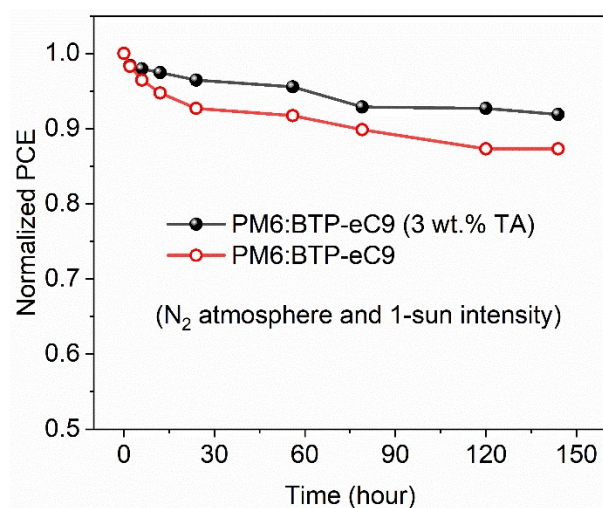
Figure S38. Normalized PCE of inverted devices of unencapsulated PM6:BTP-eC9 and 3 wt.% TA-doped PM6:BTP-eC9-based device in the glovebox with illumination of 1-sun simulator (100 mW cm^{-2}).

Table S1. Summarized parameters of the neat films with or w/o TA ordered structures.

Blend film	π-π stacking (OOP)				Lamellar stacking (IP)			
	q_z [Å^{-1}]	d_π [Å]	FWHM [Å^{-1}]	CCL [Å]	q_{xy} [Å^{-1}]	$d_{lamellar}$ [Å]	FWHM [Å^{-1}]	CCL [Å]
PM6	1.676	3.749	0.303	19.29	0.292	21.54	0.090	64.74
D18-2F	1.622	3.875	0.296	19.73	0.307	20.45	0.105	55.85
PM6:D18-2F (9:1)	1.655	3.796	0.271	21.56	0.300	20.95	0.089	65.47
BTP-eC9	1.688	3.723	0.318	18.39	0.385	16.32	0.149	39.13
PM6:D18-2F (3 wt.% TA)	1.706	3.683	0.273	21.43	0.292	21.53	0.082	71.50
BTP-eC9 (3 wt.%TA)	1.751	3.589	0.291	20.06	0.385	16.32	0.134	43.56

Table S2. Mechanical parameters of the of the neat films with or w/o TA obtained by AFM PFQNM, film on elastomer (FOE) and film on water (FOW) method.

Donor	AFM PFQNM			Film on Elastomer	Film on Water
	Elastic modulus [GPa]	Stiffness [N/m]	Compliance [×10^{-2} m/N]	COS$_{FOE}$ [%] [a]	COS$_{FOW}$ [%]

PM6	2.98	23.45	4.26	17.5	9.3
D18-2F	2.26	17.04	5.87	/	13.5
PM6:D18-2F	2.69	18.16	5.51	/	11.7
PM6:D18-2F(TA)	/	/	/	/	14.3

[a] COS_{FOE} data of PM6 film comes from our previous work (Matter, 2022, 5, 1877–1889).

Table S3. The detailed photovoltaic parameters of PM6:BTP-eC9 based device with PEDOT:PSS (4083) as HTL.

Active layer	V_{OC} [V]	J_{SC} [mA/cm^2]	FF [%]	PCE [a] [%]	R_s [Ω cm^2]	$R_{sh} \times 10^3$ [Ω cm^2]
Binary 4083 as HTL	0.849	28.00	77.9	18. 44 (18.13)	2.26	2.81

PM6:BTP-eC9=1:1.2 (w:w) blend film as photovoltaic layer, PEDOT:PSS (4083) as hole transport layer (HTL);

Table S4. The detailed photovoltaic parameters of PM6:BTP-eC9 based device doped with different concentrations of TA.

Active layer	V_{OC} [V]	J_{SC} [mA/cm^2]	FF	PCE [%]
PM6:BTP-eC9	0.851	28.58	78.27	18.97 (18.75)
PM6:BTP-eC9 (1 wt. % TA)	0.855	28.53	78.19	19.07 (18.86)
PM6:BTP-eC9 (3 wt.% TA)	0.858	28.73	78.00	19.22 (19.03)
PM6:BTP-eC9 (5 wt.% TA)	0.853	28.48	77.49	18.84 (18.52)

PM6:BTP-eC9=1:1.2 (w:w) blend film as photovoltaic layer, 4PADCB SAM as hole transport layer (HTL).

Table S5. The detailed photovoltaic parameters of PM6:D18-2F:BTP-eC9-based devices by varying the blending ratio of D18-2F.

Active layer	V_{OC} [V]	J_{SC} [mA/cm^2]	FF	PCE [%]

PM6:D18-2F:BTP-eC9 (1:0:1.2)	0.851	28.58	78.27	18.97 (18.75)
PM6:D18-2F:BTP-eC9 (0.95:0.05:1.2)	0.855	28.63	77.96	19.08 (18.84)
PM6:D18-2F:BTP-eC9 (0.9:0.1:1.2)	0.858	28.82	78.43	19.39 (19.21)
PM6:D18-2F:BTP-eC9 (0.08:0.2:1.2)	0.862	28.08	78.13	18.91 (18.57)

Donor: Acceptor=1:1.2 (w:w) blend film as photovoltaic layer, 4PADCB SAM as hole transport layer (HTL).

Table S6. Detailed parameters of binary and ternary devices for electron and hole mobilities.

Active layer	Electron mobility ($\times 10^{-4}$ cm^2 V^{-1} s^{-1})	Hole mobility ($\times 10^{-4}$ cm^2 V^{-1} s^{-1})	μ_e/μ_h
Binary	5.95	4.35	1.37
Binary (TA)	7.63	4.7	1.62
Ternary (TA)	10.9	9.62	1.13

Table S7. Surface energy characteristics of the donor and acceptor pristine films.

Surface	θ_{water}	$\theta_{CH_2I_2}$	γ^d [mN m^{-1}]	γ^p [mN m^{-1}]	γ [mN m^{-1}]	$\chi^{\text{D-A a)}}$	$\chi^{\text{D/PM6 b)}}$	ω_D[c)]
PM6	102.825°	58.912°	29.612	0.166	29.778	0.406k	/	/
D18-2F	99.148°	53.389°	32.495	0.313	32.809	0.134k	0.073k	-0.150
BTP-eC9	92.578°	45.016°	36.276	0.865	37.141	/	/	/
PM6 (TA)	100.469°	55.558°	31.347	0.260	31.608	0.223k	/	/
BTP-eC9 (TA)	90.01°	45.035°	35.569	1.433	37.002	/	/	/

[a)] The Flory-Huggins interaction parameter between the donor and acceptor is calculated through the equation of: $\chi_{D/A} = \kappa(\sqrt{\gamma_A} - \sqrt{\gamma_D})^2$.

[b)] The Flory-Huggins interaction parameter between the two acceptors (PM6 and D) is calculated through the equation of: $\chi_{D/PM6} = \kappa(\sqrt{\gamma_D} - \sqrt{\gamma_{PM6}})^2$.

[c)] The wetting coefficient (ω) of the third component D in the mixture of PM6:BTP-eC9 is calculated according to Young's equation: $\omega_D = \dfrac{\chi_{BTP-eC9/D} - \chi_{PM6/D}}{\chi_{PM6/BTP-eC9}}$.

Table S8. Summarized parameters of the blend films with or w/o TA ordered structures.

Blend film	π-π stacking (OOP)				Lamellar stacking (IP)			
	q_z [Å^{-1}]	d_π [Å]	FWHM [Å^{-1}]	CCL [Å]	q_{xy} [Å^{-1}]	$d_{lamellar}$ [Å]	FWHM [Å^{-1}]	CCL [Å]
PM6:BTP-eC9	1.727	3.639	0.279	20.94	0.304	20.69	0.153	38.24
PM6:BTP-eC9 (TA)	1.721	3.650	0.249	23.51	0.308	20.43	0.144	40.45
PM6:D18-2F:BTP-eC9 (TA)	1.711	3.672	0.249	23.46	0.304	20.69	0.147	39.81

Table S9. Detailed parameters of binary and ternary devices for electron and hole mobilities.

	COS$_{FOW}$ [%]	Highest stress [MPa]	Stiffness [N/m]
PM6:BTP-eC9	3.63	13.93	26.11
PM6:BTP-eC9 (TA)	5.51	32.50	22.35
PM6:D18-2F:BTP-eC9 (TA)	6.44	39.28	18.19

Table S10. Comparisons of PCE values of plastic substrate-based flexible devices in the recent years.

Year	Active layer	PCE (%)	Refer.
2019	Front cell: PBDB-T:F-M Rear cell: PTB7-Th:PC$_{71}$BM:O6T-4F	16.55	[2]
2020	PM6:Y6	15.20	[3]
2020	PM6:Y6	15.03	[4]
2020	PM6:Y6	15.12	[5]
2020	PM6:Y6	15.21	[6]
2020	PM6:N3:PC$_{71}$BM	16.10	[7]
2021	D18-Cl:G19:Y6	15.90	[8]
2021	PM6:BTP-eC9	16.00	[9]
2021	PM6:Y6	16.61	[10]
2022	PM6:BTP-eC9	16.71	[11]
2022	PM6:BTP-eC9:PY-IT	16.52	[12]
2022	PM6:BTP-eC9:PC71BM	17.50	[13]
2023	PM6:L8-BO	17.40	[14]
2023	D18:N3:DOY-TVT	18.06	[15]
2024	D18:Y6:PC$_{71}$BM	18.00	[16]
2024	PM6:L8-BO	18.05	[17]

| 2024 | PM6:D18-2F:BTP-eC9 | 18.32 | **This work** |

Supplemental References

1. J. Xue, H. Zhao, C. Zhao, L. Tang, Y. Wang, J. Xin, Z. Bi, K. Zhou and W. Ma, *Adv. Funct. Mater.*, 2023, **33**, 2303403.

2. Y. Sun, M. Chang, L. Meng, X. Wan, H. Gao, Y. Zhang, K. Zhao, Z. Sun, C. Li, S. Liu, H. Wang, J. Liang and Y. Chen, *Nature Electronics*, 2019, **2**, 513-520.

3. D. Koo, S. Jung, J. Seo, G. Jeong, Y. Choi, J. Lee, S. M. Lee, Y. Cho, M. Jeong, J. Lee, J. Oh, C. Yang and H. Park, *Joule*, 2020, **4**, 1021-1034.

4. F. Qin, W. Wang, L. Sun, X. Jiang, L. Hu, S. Xiong, T. Liu, X. Dong, J. Li, Y. Jiang, J. Hou, K. Fukuda, T. Someya and Y. Zhou, *Nat. Commun.*, 2020, **11**, 4508.

5. J. Kim, D. Ouyang, H. Lu, F. Ye, Y. Guo, N. Zhao and W. C. H. Choy, *Adv. Energy Mater.*, 2020, **10**, 1903919.

6. X. Chen, G. Xu, G. Zeng, H. Gu, H. Chen, H. Xu, H. Yao, Y. Li, J. Hou and Y. Li, *Adv. Mater.*, 2020, **32**, e1908478.

7. T. Y. Qu, L. J. Zuo, J. D. Chen, X. L. Shi, T. Zhang, L. Li, K. C. Shen, H. Ren, S. Wang, F. M. Xie, Y. Q. Li, A. K. Y. Jen and J. X. Tang, *Advanced Optical Materials*, 2020, **8**, 2000669.

8. Z. Chen, W. Song, K. Yu, J. Ge, J. Zhang, L. Xie, R. Peng and Z. Ge, *Joule*, 2021, **5**, 2395-2407.

9. X. Song, G. Liu, P. Sun, Y. Liu and W. Zhu, *J Phys Chem Lett*, 2021, **12**, 10616-10621.

10. J. Wan, Y. Xia, J. Fang, Z. Zhang, B. Xu, J. Wang, L. Ai, W. Song, K. N. Hui, X. Fan and Y. Li, *Nano-micro letters*, 2021, **13**, 44.

11. X. Liu, Z. Zheng, J. Wang, Y. Wang, B. Xu, S. Zhang and J. Hou, *Adv. Mater.*, 2022, **34**,

e2106453.

12. W. Song, K. Yu, J. Ge, L. Xie, R. Zhou, R. Peng, X. Zhang, M. Yang, Z. Wei and Z. Ge, *Matter*, 2022, **5**, 1877-1889.

13. G. Zeng, W. Chen, X. Chen, Y. Hu, Y. Chen, B. Zhang, H. Chen, W. Sun, Y. Shen, Y. Li, F. Yan and Y. Li, *J. Am. Chem. Soc.*, 2022, **144**, 8658-8668.

14. X. J. Zheng, L. J. Zuo, K. R. Yan, S. Q. Shan, T. Y. Chen, G. Y. Ding, B. W. Xu, X. Yang, J. H. Hou, M. M. Shi and H. Z. Chen, *Energy Environ. Sci.*, 2023, **16**, 2284-2294.

15. W. Song, Q. Ye, S. Yang, L. Xie, Y. Meng, Z. Chen, Q. Gu, D. Yang, J. Shi and Z. Ge, *Angew. Chem. Int. Ed. Engl.*, 2023, **62**, e202310034.

16. H. Ren, W.-S. Chen, J.-D. Chen, J.-P. Yang, Y.-F. Zhang, H.-Y. Hou, S. Tian, H.-R. Ge, Y.-Q. Li and J.-X. Tang, *Chem. Eng. J.*, 2024, **481**, 148498.

17. Z. Xiao, S. Li, J. Liu, X. Chen, Z. Suo, C. Li, X. Wan and Y. Chen, *Solar RRL*, 2024, DOI: 10.1002/solr.202400206, 2400206.